Check for updates

Batteries & Supercaps

Research Article
doi.org/10.1002/batt.202400779

Chemistry Europe
European Chemical Societies Publishing

www.batteries-supercaps.org

Composite (bi-)metallic oxides with heterostructure and heteroatom-doped porous carbon as advanced potassium-ion battery anodes

Junqi Wang[+],[b] Peng Wu[+],[b] Ke Wang,[a] Yiren Zhong,[a] Gaoming Sun,[b] Yuanchun Ji,*[c] Yuan Ma,*[a] and Yanjiao Ma*[b]

In this work, a scalable two-step synthesis method was employed to develop transition metal oxide/carbon composites that exhibit excellent electrochemical performance as the anode of potassium-ion batteries. The functionalized metal-organic framework precursor was combined with molecular silicotungstic acid clusters (SiW9) during thermal conversion, and embedded into in-situ formed porous carbon matrix to form a multi-component $CoWO_4/WO_3$-C composite material with N-doping. Benefiting from unique compositional and structural features, the resulting composite exhibits an appealing potassium-ion storage performance, such as, large specific capacity of ca. 1500 mAh/g after 600 cycles and excellent rate capability, i.e., delivering reversible capacity over 200 mAh/g even at the high-rate of 2.0 A/g.

Introduction

To address growing environmental challenges and the dwindling supply of fossil fuels, scientists and engineers are dedicated to advancing highly efficient energy storage technologies that support greener and more sustainable energy solutions.[1–3] In this context, lithium-ion batteries (LIBs) are crucial as energy sources for next-generation electric vehicles and portable electronics, including smartphones, laptops, and smart glasses.[4–6] However, the large-scale application of LIBs in energy storage is hindered by the high cost of lithium, its limited reserves, and uneven distribution.[7–9] Given the abundant and evenly distributed potassium metal resources, along with its low production cost and more negative redox potential (−2.93 V vs. standard hydrogen electrode), potassium-ion batteries (PIBs) are emerging as a promising candidate for the next generation of energy storage systems due to their similar electrochemical storage mechanisms to LIBs.[10–12] In the initial stages of PIB development, many active materials of LIBs can be referenced and directly applied to potassium-ion storage. For example, commercial graphite can effectively store and release potassium ions through de-/insertion mechanism, with a reversible capacity of up to 273 mAh/g.[13]

Transition metal oxides (TMOs) are another extensively studied as anode materials due to their high theoretical capacities (such as, Fe_2O_3: 1007 mAh/g, Co_3O_4: 890 mAh/g).[14,15] These impressive capacities result from the multi-electron transfer mechanism involved in the conversion reaction.[16] However, applying as anode materials, TMOs face several challenges: i) low electronic conductivity leads to sluggish reaction kinetics and poor rate performance; ii) large volume variation during repeated dis-/charge process cause structural degradation and cycling degradation.[17,18] To overcome these issues, researchers have developed various performance optimization strategies that can be broadly categorized into compositional and structural approach. The former include carbon coating, heteroatom doping, and composite design, while the latter focus on engineering nano-, hetero-, and porous structures.[14,19–22] These approaches effectively preserve the structural integrity of TMOs and enhance ion/electron transport during cell operation.[23,24] However, the development of anode materials with multiple components and complex structural features often requires intricate and time-consuming preparation processes, which significantly hinder their scalability for practical applications. Thus, there is a pressing need for simple, efficient, and universal preparation methods to streamline the synthesis process and enable broader implementation.[25,26]

A promising approach to developing advanced anode materials with optimized structural and compositional attributes involves the strategic design of precursors. Hybrid systems that combine metal-organic frameworks (MOFs) with polyoxometalates (POMs) have garnered attention due to their unique advantages.[27,28] Through a straightforward post-treatment, the metal centers and organic ligands in MOFs can transform *in situ* into porous carbon-coated metal oxide nanocomposites with heteroatom doping.[29–31] Integrating molecular-scale POMs into

[a] *K. Wang, Y. Zhong, Y. Ma*
Confucius Energy Storage Lab, Key Laboratory of Energy Thermal Conversion and Control of Ministry of Education, School of Energy and Environment & Z Energy Storage Center, Southeast University, Nanjing 211189, China
E-mail: mayuan_chem@outlook.com

[b] *J. Wang,[+] P. Wu,[+] G. Sun, Y. Ma*
School of Energy and Mechanical Engineering, Nanjing Normal University, Nanjing 210023, China
E-mail: yanjiao.ma@njnu.edu.cn

[c] *Y. Ji*
Contemporary Amperex Technology Co., Limited, China
E-mail: yuanchun.ji@qq.com

[+] *These authors contribute equally.*

Supporting information for this article is available on the WWW under https://doi.org/10.1002/batt.202400779

© 2025 Wiley-VCH GmbH

MOFs (POM@MOF), where the particle size of the POMs is compatible with the MOF cavity, further broadens the structural and chemical diversity of the derived materials.[32,33]

Our previous research introduced this concept by demonstrating the synthesis of {V_{10}}@ZIF-67 derivatives, which exhibited superior electrochemical energy storage performance.[34] Expanding on this idea, we incorporated {SiW_9} into ZIF-67 cavities and synthesized a novel composite material through a one-step carbonization process. The resulting material consists of Co–W oxide nanoparticles embedded in N-doped carbon frameworks (denoted as CWO@N–C). When evaluated as an anode material for potassium-ion batteries, the CWO@N–C composite achieved remarkable electrochemical performance, including high reversible capacity, excellent long-term cycling stability, and superior rate capability.

Results and Discussion

The resulting composite (CWO@N–C) was synthesized through a two-step process (Scheme 1). First, the POM@MOF precursor was prepared by co-precipitating {SiW_9}, Co(II), and 2-methylimidazole in methanol. In the second step, the precursor underwent a post-annealing treatment, as detailed in the Experimental Section. Powder X-ray diffraction (XRD) analysis provided structural insights into CWO@N–C. The diffraction pattern (Figure 1a) predominantly displayed peaks corresponding to $CoWO_4$ (JCPDS card No. 15–0867) and WO_3 (JCPDS card No. 32–1394). The quasi-surface composition of CWO@N–C was further investigated via X-ray photoelectron spectroscopy (XPS). The C 1s detailed spectrum (Figure 1b) shows three peaks at 284.8, 286.3, 288.4 eV, assigning to C=C/C–C/C–H, C–O/C–N, and O=C–O species, respectively.[35] The high-resolution N 1s spectrum (Figure 1c) confirmed the presence of pyrrolic-N (400.1 eV) and pyridinic-N (398.2 eV) within the carbon matrix.[34,36,37] For tungsten, the W 4f spectrum (Figure 1d) shows two distinct peaks at approximately 37.9 and 35.6 eV, indicative of W(VI).[38,39] Meanwhile, the Co 2p spectrum (Figure 1e) features two prominent peaks at ca. 780.7 eV (Co $2p_{3/2}$) and 796.5 eV (Co $2p_{1/2}$), accompanied by satellite peaks, characteristic of Co(II).[14,40] Additionally, the O 1s spectrum (Figure S1) can be deconvoluted into two peaks, with one at ~530 eV corresponding to metal–O bonds, specifically Co–W oxides. By analyzing the XPS survey spectrum(Figure S2), a characteristic Si 2 s peak was detected at 167.7 eV, indicating the presence of a tiny amount of silicon in the material (Table S1).[41] These findings indicate that the POM@MOF precursor was almost entirely converted into a mixed Co–W oxide system containing various N- and O-modified carbon species.[21]

Scanning electron microscopy (SEM) and transmission electron microscopy (TEM) were utilized to examine the morphology and microstructure of the POM@MOF precursor and CWO@N–C composites, as shown in Figure 2. The as-prepared hybrid precursor displayed a quasi-polyhedral microstructure with an approximate size of 100 nm. Notably, the incorporation of POM@MOF polyhedrons resulted in a transition from smooth to rough surface textures (Figure 2a-b).[42] After annealing, the CWO@N–C composites retained the initial quasi-polyhedral morphology, albeit with rougher surfaces. This enhanced surface roughness is advantageous for achieving a larger surface area and providing more potassium ion storage sites (Figure 2c-d).[43] The internal structure of the CWO@N–C composites was further elucidated using TEM (Figure 2d-f). Low-magnification TEM images (Figure 2d) revealed quasi-polyhedral frameworks with various porous structures. These porous features likely resulted from the release of gaseous products (e.g., CO_2, H_2O, and CO) during the annealing process, which escaped from the interior of the POM@MOF precursor.[22,44] Importantly, high-resolution TEM images (Figure 2e-f) clearly showed crystalline particles embedded within

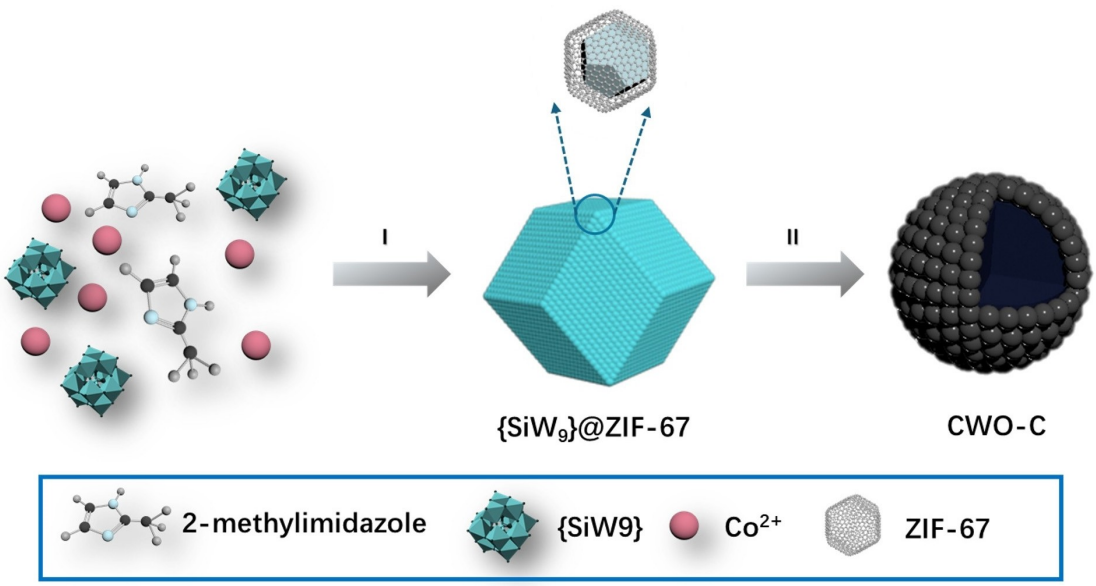

Scheme 1. Illustration of the two-step fabrication process of the CWO@N–C composite.

© 2025 Wiley-VCH GmbH

25666223, 2025, 8, Downloaded from https://chemistry-europe.onlinelibrary.wiley.com/doi/10.1002/batt.202400779 by University of Ulsan, Wiley Online Library on [11/11/2025]. See the Terms and Conditions (https://onlinelibrary.wiley.com/terms-and-conditions) on Wiley Online Library for rules of use; OA articles are governed by the applicable Creative Commons License

Research Article
doi.org/10.1002/batt.202400779
Chemistry Europe
European Chemical Societies Publishing

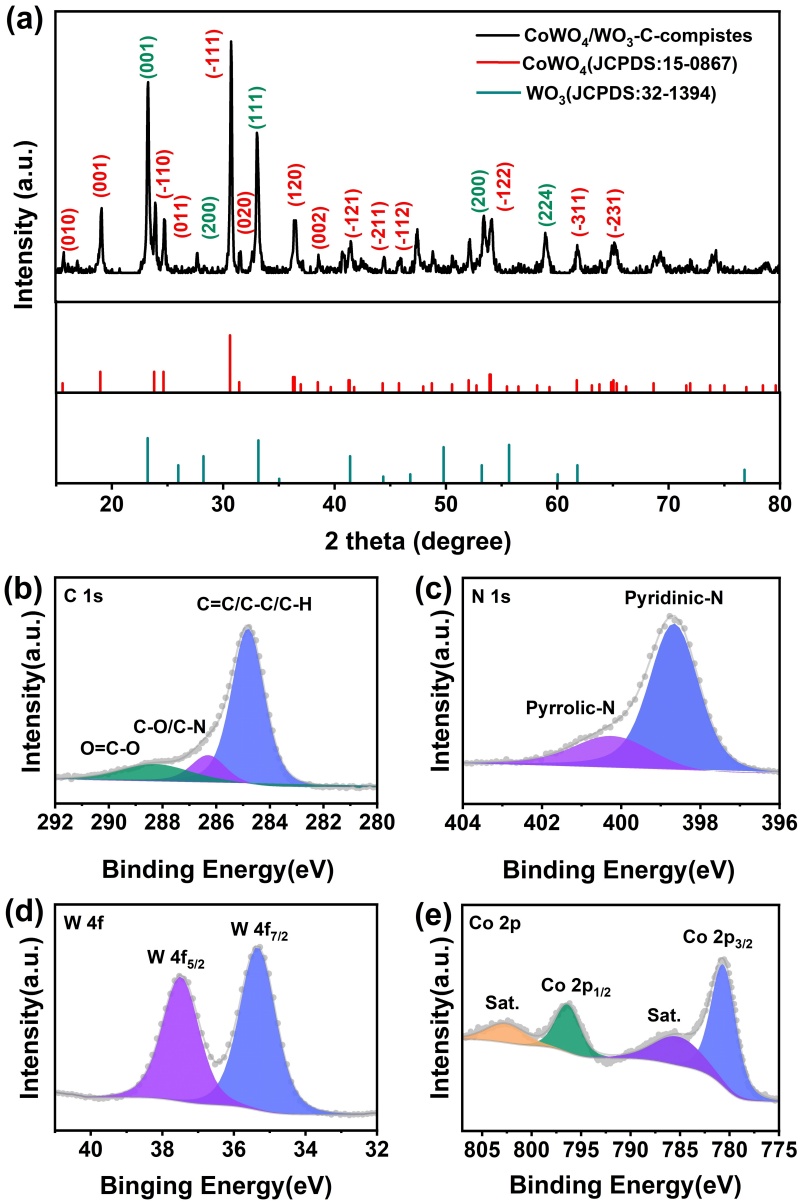

Figure 1. (a) XRD pattern of CWO@N–C compistes and high-resolution XPS spectra of the (b) C 1s, (c) N 1s, (d) W 4f, and (e) Co 2p regions for CWO@N–C composites.

the carbon matrix. Among these, interlayer distances of 0.246, 0.243, and 0.220 nm corresponded to the (120), (021), and (−121) lattice planes of $CoWO_4$, respectively. Additionally, interlayer distance of 0.208 nm was attributed to the (111) lattice plane of WO_3. Overall, SEM and TEM analyses demonstrated that the CWO@N–C composites exhibit a microscale quasi-polyhedral morphology, with Co–W oxide nanoparticles encapsulated by graphitic carbon and anchored within a porous carbonaceous matrix.

The potassium-ion storage performance of CWO@N–C composites was evaluated using coin cells, with the results summarized in Figure 3. The composites demonstrated a high reversible capacity of approximately 400 mAh/g at a current density of 100 mA/g after the initial charge process (Figure 3a). However, the initial coulomb efficiency was relatively low (66.8 %), likely due to the composite's large surface area, porous structure and active defects.[7,45] In general, pre-potassium treatment and electrolyte engineering are promising strategies to address this issue, as they can replenish K-ions and/or regulate SEI formation, thereby improving the initial coulomb efficiency.[46,47] During subsequent galvanostatic charge/discharge tests, the CWO@N–C electrode exhibited stale cycling performance over the first 10 cycles (Figure 3a). Notably, the specific capacity gradually increased, exceeding 1500 mAh/g by the 600th cycle (Figure 3c). The phenomenon of initial cycling capacity enhancement was analyzed through the charge–discharge profiles presented in Figure 3b. It was observed that the capacity increase primarily originates from the synergistic contribution of the discharge process at low potentials (<0.8 V vs. K^+/K) and the charge process at high potentials (>2.3 V vs.

© 2025 Wiley-VCH GmbH

25666223, 2025, 8, Downloaded from https://chemistry-europe.onlinelibrary.wiley.com/doi/10.1002/batt.202400779 by University of Ulsan, Wiley Online Library on [11/11/2025]. See the Terms and Conditions (https://onlinelibrary.wiley.com/terms-and-conditions) on Wiley Online Library for rules of use; OA articles are governed by the applicable Creative Commons License

Research Article
doi.org/10.1002/batt.202400779
Chemistry Europe
European Chemical Societies Publishing

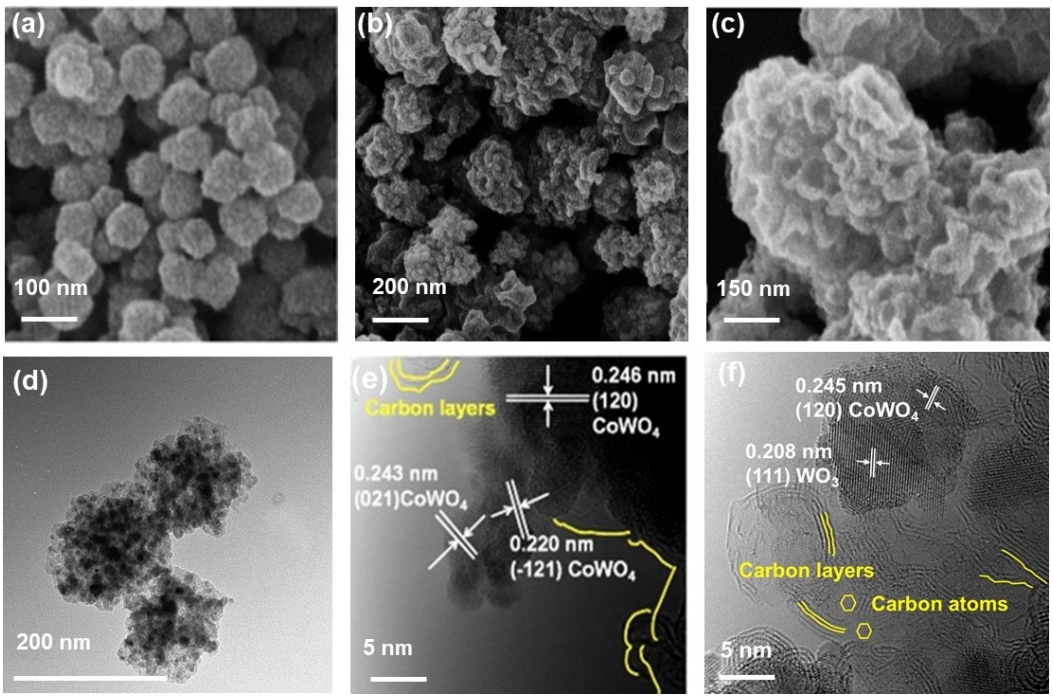

Figure 2. SEM images of (a) POM@MOF polyhedrons and (b,c) CWO@N–C composites. (HR)TEM images of (d-f) CWO@N–C.

K^+/K).This capacity growth is primarily attributed to the formation of "quasi-reversible" solid electrolyte interphases (SEIs), a phenomenon previously observed in other conversion-based materials.[48,49] During the first discharge, electrolyte decomposition occurs at low potentials (<0.8 V vs. K^+/K), leading to the formation of an SEI layer on the electrode surface. Some components of the SEI undergo reversible transformations during subsequent charge–discharge cycles, contributing to the additional capacity. The surface roughness and porosity of the electrode directly influence the kinetics of SEI formation, with a higher specific surface area accelerating electrolyte decomposition and resulting in a thicker SEI layer. However, this also facilitates rapid K^+ diffusion at the interface. This competing effect enhances the utilization of active materials during the initial cycles, resulting in higher capacity compared to later cycles. As cycling progresses, the SEI layer gradually restructures into a denser form, reducing its redox activity and stabilizing the capacity.[22,50,51] The evolution of the SEIs is supported by the voltage profiles recorded between the 20th and 200th cycles (Figure 3b).[52–54] The rate performance of the CWO@N–C composites is illustrated in Figure 3d-e. The electrode delivered average specific capacities of 400, 350, 320, 250, 200, 180, and 150 mAh/g at current densities of 50, 100, 200, 500, 1000, 1500, and 2000 mA/g, respectively. When the current density was returned to 50 mA/g, the specific capacity exceeded 400 mAh/g, demonstrating the composite's excellent cycling stability and rate capability. Overall, the CWO@N–C composites exhibited superior potassium-ion storage properties compared to previously reported conversion-based electrode materials, as summarized in Table S2.

To further investigate the promising rate capability of CWO@N–C composites, kinetic analysis was conducted using cyclic voltammetry (CV) at scan rates ranging from 0.1 to 2.0 mV/s (Figure 4a). The CV curves retained similar shapes with minimal peak shifts as the scan rate increased, indicating fast K-ion storage kinetics, consistent with the rate performance results. The degree of (pseudo−)capacitive contribution was quantified by analyzing the relationship between the measured peak current (i) and the scan rate (v) using the equations:[42,55]

$$i = av^b \tag{1}$$

$$\log i = b\log v + \log a \tag{2}$$

Here, a is a constant, and b is derived from the slope of the log(i) versus log(v) plot. A b-value of 1.0 indicates capacitive-controlled behavior, while a b-value of 0.5 signifies a diffusion-controlled process.[56] Based on the fitted line (Figure 4b), the calculated b-value for CWO@N–C composites was 0.85 and 0.94, suggesting that the charge-transfer kinetics are primarily governed by the pseudocapacitive mechanism.

To more precisely quantify the capacitive contribution, the current response i(V) at a given potential V was deconvoluted into capacitive (k_1v) and diffusion-controlled ($k_2v^{1/2}$) components using the equation:[42]

$$i(\mathrm{V}) = k_1v + k_2v^{1/2}$$

Here, k_1 and k_2 are constants at a specific potential. By plotting i(V)/$v^{1/2}$ against $v^{1/2}$, the slope and intercept represent the k_1 and k_2 values, respectively. Figure 4c shows the analysis

© 2025 Wiley-VCH GmbH

25666223, 2025, 8, Downloaded from https://chemistry-europe.onlinelibrary.wiley.com/doi/10.1002/batt.202400779 by University of Ulsan, Wiley Online Library on [11/11/2025]. See the Terms and Conditions (https://onlinelibrary.wiley.com/terms-and-conditions) on Wiley Online Library for rules of use; OA articles are governed by the applicable Creative Commons License

Research Article
doi.org/10.1002/batt.202400779
Chemistry Europe
European Chemical Societies Publishing

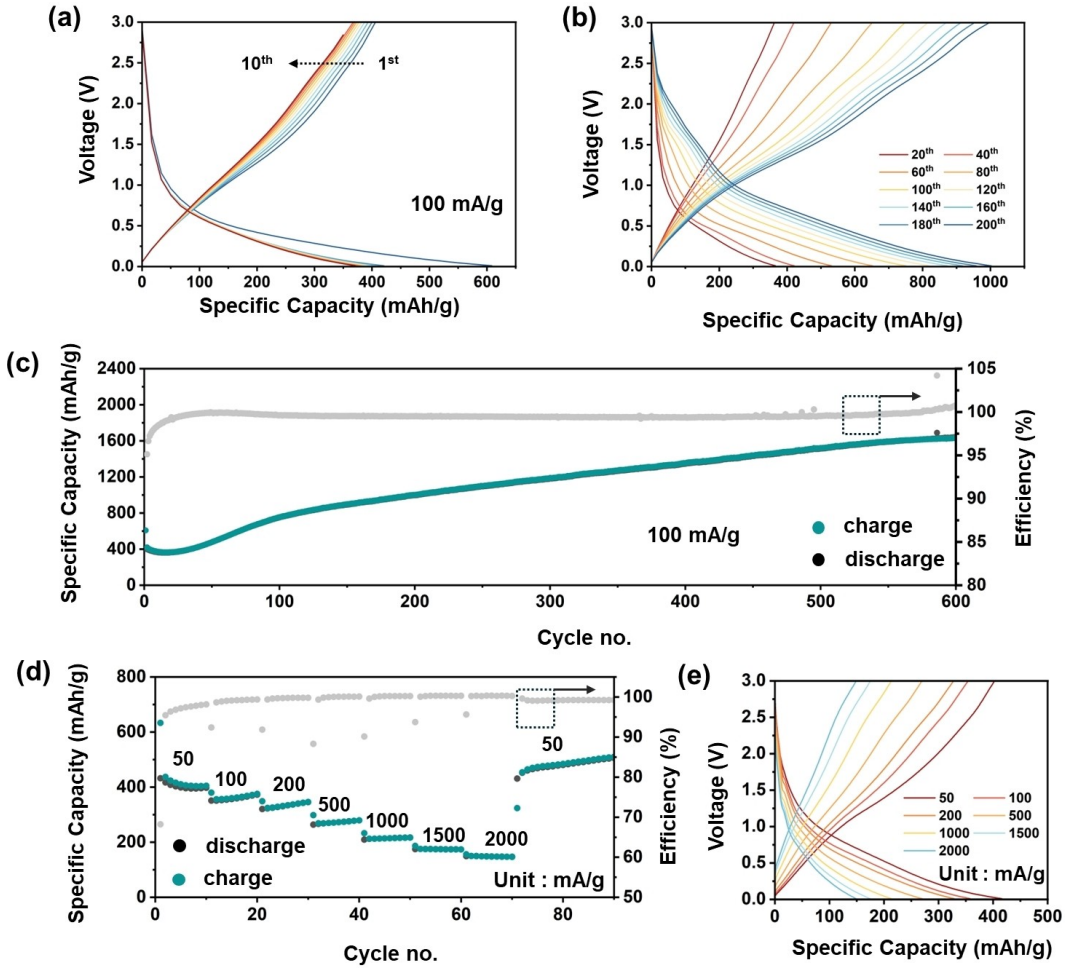

Figure 3. Potassium-ion storage performance of CWO@N–C electrodes: (a) dis-/charge voltage profiles for the first ten galvanostatic cycles at a specific current of 100 mA/g; (b) selected dis-/charge voltage profiles from 20th to 200th cycles at a specific current of 100 mA/g; (c) 'capacity vs. cycle number' plot for 600 galvanostatic cycles, applying a constant specific current of 100 mA/g; (d) rate capability test, applying various specific currents ranging from 50 to 2000 mA/g for 90 cycles in total; (e) rate performance voltage profiles for the 5th (50 mA/g), 15th (100 mA/g), 25th (200 mA/g), 35th (500 mA/g), 45th (1000 mA/g), 55th (1500 mA/g), and 65th (2000 mA/g).

results at a scan rate of 1.0 mV/s, where 88.7% of the total charge was attributed to the (pseudo−)capacitive contribution. Figure 4d shows the pseudo-capacitive contributions at scan rates ranging from 0.1 to 2.0 mV/s. As expected, the (pseudo−)capacitive contribution increases with the scan rate. At a scan rate of 2.0 mV/s, the pseudo-capacitive contribution reaches 93.4%. This significant (pseudo−)capacitive contribution can be attributed to the composite's large specific surface area and porous structure, further supporting its excellent rate performance.

Conclusions

By strategically designing the POM@MOF precursor, an advanced composite comprising a Co–W oxide heterosystem embedded within an N-doped carbonaceous framework was successfully synthesized through a straightforward post-annealing treatment. The resulting composite exhibited multiple structural and compositional advantages, including nanoscale active particles, heteroatom doping, a porous structure, and a large surface area. As a result, the CWO@N–C composite demonstrated outstanding potassium-ion storage performance. It achieved excellent cycling stability, with a high reversible capacity of 1500 mAh/g after 600 cycles, as well as impressive rate capability. The findings presented in this work establish a robust research paradigm for designing advanced electrode materials and are expected to drive the development of high-performance potassium-ion batteries.

Acknowledgements

This work is supported by the Project on Carbon Emission Peak and Neutrality of Jiangsu Province (No. BE2022031-4), a Research Start-up Fund of Southeast University (RF1028624081) and a Research Start-up Fund of Nanjing Normal University (184080H201B41). This work is financially supported by the Fundamental Research Funds for the Central Universities (No. 2242024K30047)

© 2025 Wiley-VCH GmbH

25666223, 2025, 8, Downloaded from https://chemistry-europe.onlinelibrary.wiley.com/doi/10.1002/batt.202400779 by University of Ulsan, Wiley Online Library on [11/11/2025]. See the Terms and Conditions (https://onlinelibrary.wiley.com/terms-and-conditions) on Wiley Online Library for rules of use; OA articles are governed by the applicable Creative Commons License

Research Article
doi.org/10.1002/batt.202400779
Chemistry Europe
European Chemical Societies Publishing

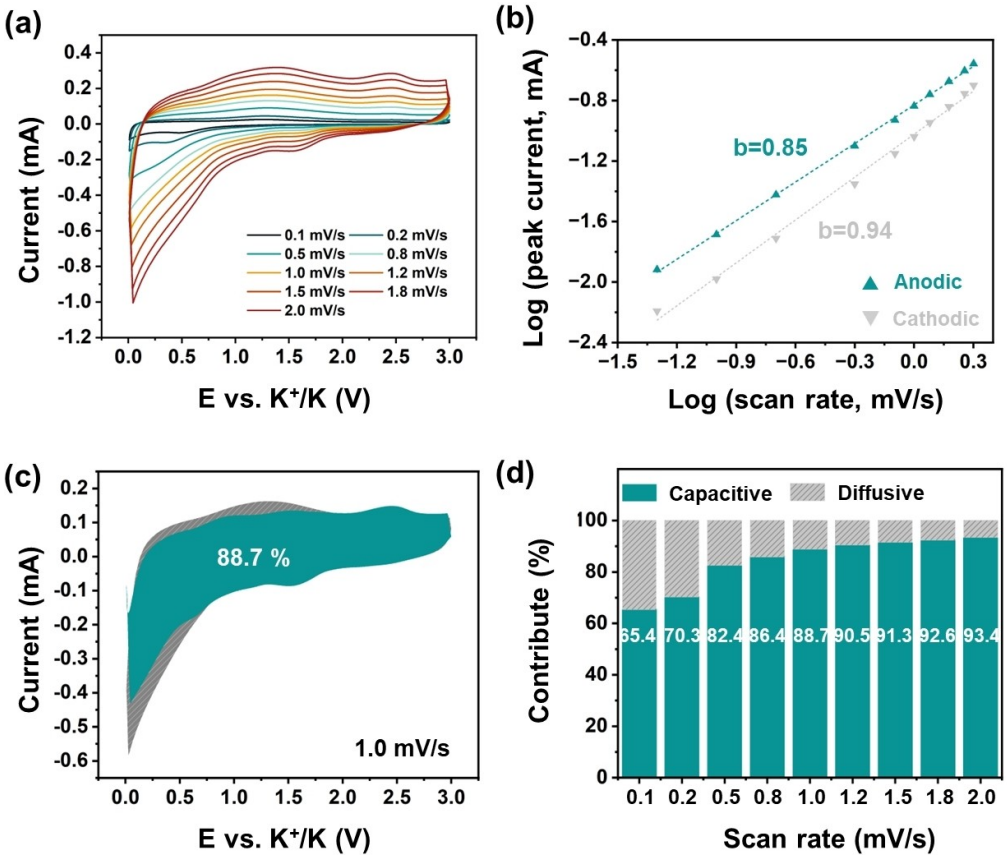

Figure 4. Kinetic analysis of the K-ion storage: (a) CV curves at different sweep rates; (b) calculation of the *b*-value (see Eq (1) and (2)) by plotting the logarithmic peak current (log *i*) vs. the logarithm of the applied scan rate (log *v*); (c) illustration of the pseudocapacitive (green area) and diffusion-controlled (gray area) contributions to the overall charge storage, exemplarily depicted for a scan rate of 1.0 mV/s; (d) The percentage of the (pseudo−)capacitive contribution with scan rate from 0.1 mV/s-2.0 mV/s.

Conflict of Interests

The authors declare no conflict of interest.

Data Availability Statement

The data that support the findings of this study are available from the corresponding author upon reasonable request.

[1] C. Zhang, H. Zhao, Y. Lei, *Energy Environ. Mater.* **2020**, *3*, 105.
[2] Y. Yue, H. Liang, *Adv. Energy Mater.* **2017**, *7*, 1602545.
[3] W. Ai, Z. Luo, J. Jiang, J. Zhu, Z. Du, Z. Fan, L. Xie, H. Zhang, W. Huang, T. Yu, *Adv. Mater.* **2014**, *26*, 6186.
[4] A. Yoshino, *Angew. Chem. Int. Ed.* **2012**, *51*, 5798.
[5] G. Fang, J. Zhou, C. Liang, A. Pan, C. Zhang, Y. Tang, X. Tan, J. Liu, S. Liang, *Nano Energy* **2016**, *26*, 57.
[6] Y. Ma, Z. Zhou, T. Brezesinski, Y. Ma, Y. Wu, *Research* **2024**, *7*, 0503.
[7] C. Liu, S. Luo, H. Huang, Y. Zhai, Z. Wang, *ChemSusChem* **2019**, *12*, 873.
[8] D. Wu, X. Li, B. Xu, N. Twu, L. Liu, G. Ceder, *Energy Environ. Sci.* **2015**, *8*, 195.
[9] S. Liu, L. Kang, J. Henzie, J. Zhang, J. Ha, M. A. Amin, M. S. A. Hossain, S. C. Jun, Y. Yamauchi, *ACS Nano* **2021**, *15*, 18931.
[10] Y. Liu, Q. Deng, Y. Li, Y. Li, W. Zhong, J. Hu, X. Ji, C. Yang, Z. Lin, K. Huang, *ACS Nano* **2021**, *15*, 1121.
[11] R. Huang, J. Lin, J. Zhou, E. Fan, X. Zhang, R. Chen, F. Wu, L. Li, *Small* **2021**, *17*, 2007597.
[12] Y. Ma, Y. Ma, H. Euchner, X. Liu, H. Zhang, B. Qin, D. Geiger, J. Biskupek, A. Carlsson, U. Kaiser, A. Groß, S. Indris, S. Passerini, D. Bresser, *ACS Energy Lett.* **2021**, *6*, 915.
[13] Z. Jian, W. Luo, X. Ji, *J. Am. Chem. Soc.* **2015**, *137*, 11566.
[14] H. Liang, Y. Zhang, S. Hao, L. Cao, Y. Li, Q. Li, D. Chen, X. Wang, X. Guo, H. Li, *Energy Storage Mater.* **2021**, *40*, 250.
[15] X. Xu, R. Cao, S. Jeong, J. Cho, *Nano Lett.* **2012**, *12*, 4988.
[16] S. Fang, D. Bresser, S. Passerini, *Adv. Energy Mater.* **2020**, *10*, 1902485.
[17] X. Niu, Y. Zhang, L. Tan, Z. Yang, J. Yang, T. Liu, L. Zeng, Y. Zhu, L. Guo, *Energy Storage Mater.* **2019**, *22*, 160.
[18] G. Huang, F. Zhang, X. Du, Y. Qin, D. Yin, L. Wang, *ACS Nano* **2015**, *9*, 1592.
[19] H. Yan, Y. Luo, X. Xu, L. He, J. Tan, Z. Li, X. Hong, P. He, L. Mai, *ACS Appl. Mater. Interfaces* **2017**, *9*, 27707.
[20] Y. Lu, L. Yu, M. Wu, Y. Wang, X. W. (David) Lou, *Adv. Mater.* **2018**, *30*, 1702875.
[21] Y. Ma, Y. Ma, D. Geiger, U. Kaiser, H. Zhang, G.-T. Kim, T. Diemant, R. J. Behm, A. Varzi, S. Passerini, *Nano Energy* **2017**, *42*, 341.
[22] Y. Ma, Y. Ma, T. Diemant, K. Cao, U. Kaiser, R. J. Behm, A. Varzi, S. Passerini, *ChemElectroChem* **2021**, *8*, 918.
[23] F. Xiao, X. Song, Z. Li, H. Zhang, L. Zhang, G. Lei, Q. Xiao, Z. Hu, Y. Ding, *J. Mater. Chem. A* **2017**, *5*, 17432.
[24] X. Gao, J. Wang, D. Zhang, K. Nie, Y. Ma, J. Zhong, X. Sun, *J. Mater. Chem. A* **2017**, *5*, 5007.
[25] Z. Lv, H. Xu, W. Xu, B. Peng, C. Zhao, M. Xie, X. Lv, Y. Gao, K. Hu, Y. Fang, W. Dong, F. Huang, *Adv. Energy Mater.* **2023**, *13*, 2300790.
[26] L. Zhang, W. (Alex) Wang, S. Lu, Y. Xiang, *Adv. Energy Mater.* **2021**, *11*, 2003640.
[27] H. B. Wu, B. Y. Xia, L. Yu, X.-Y. Yu, X. W. Lou, *Nat. Commun.* **2015**, *6*, 6512.
[28] C. Chen, A. Wu, H. Yan, Y. Xiao, C. Tian, H. Fu, *Chem. Sci.* **2018**, *9*, 4746.
[29] Y. V. Kaneti, J. Tang, R. R. Salunkhe, X. Jiang, A. Yu, K. C. -W Wu, Y. Yamauchi, *Adv. Mater.* **2017**, *29*, 1604898.

© 2025 Wiley-VCH GmbH

25666223, 2025, 8, Downloaded from https://chemistry-europe.onlinelibrary.wiley.com/doi/10.1002/batt.202400779 by University of Ulsan, Wiley Online Library on [11/11/2025]. See the Terms and Conditions (https://onlinelibrary.wiley.com/terms-and-conditions) on Wiley Online Library for rules of use; OA articles are governed by the applicable Creative Commons License

[30] F. Zheng, Y. Yang, Q. Chen, *Nat. Commun.* **2014**, *5*, 5261.
[31] X. Cao, B. Zheng, W. Shi, J. Yang, Z. Fan, Z. Luo, X. Rui, B. Chen, Q. Yan, H. Zhang, *Adv. Mater.* **2015**, *27*, 4695.
[32] Y. Ji, L. Huang, J. Hu, C. Streb, Y.-F. Song, *Energy Environ. Sci.* **2015**, *8*, 776.
[33] R. Liu, G. Zhang, H. Cao, S. Zhang, Y. Xie, A. Haider, U. Kortz, B. Chen, N. S. Dalal, Y. Zhao, L. Zhi, C.-X. Wu, L.-K. Yan, Z. Su, B. Keita, *Energy Environ. Sci.* **2016**, *9*, 1012.
[34] Y. Ji, Y. Ma, R. Liu, Y. Ma, K. Cao, U. Kaiser, A. Varzi, Y.-F. Song, S. Passerini, C. Streb, *J. Mater. Chem. A* **2019**, *7*, 13096.
[35] Y. Ma, Y. Ma, G. Kim, T. Diemant, R. J. Behm, D. Geiger, U. Kaiser, A. Varzi, S. Passerini, *Adv. Energy Mater.* **2019**, *9*, 1902077.
[36] D. Adekoya, X. Gu, M. Rudge, W. Wen, C. Lai, M. Hankel, S. Zhang, *Adv. Funct. Mater.* **2018**, *28*, 1803972.
[37] Y. Gao, Z. Han, S. Hong, T. Wu, X. Li, J. Qiu, Z. Sun, *ACS Appl. Energy Mater.* **2019**, *2*, 6071.
[38] P. Li, X. Li, Z. Zhao, M. Wang, T. Fox, Q. Zhang, Y. Zhou, *Electrochimica Acta* **2016**, *192*, 148.
[39] W.-J. Li, Z.-W. Fu, *Appl. Surf. Sci.* **2010**, *256*, 2447.
[40] S. S. Patil, U. M. Chougale, R. K. Kambale, V. J. Fulari, *J. Energy Storage* **2023**, *67*, 107517.
[41] F. Ghorban, A. Eshaghi, *Opt. Quantum Electron.* **2017**, *49*, 67.
[42] Y. Ma, Y. Ma, D. Bresser, Y. Ji, D. Geiger, U. Kaiser, C. Streb, A. Varzi, S. Passerini, *ACS Nano* **2018**, *12*, 7220.
[43] Z.-S. Wu, W. Ren, L. Xu, F. Li, H.-M. Cheng, *ACS Nano* **2011**, *5*, 5463.
[44] L. Zhang, H. B. Wu, S. Madhavi, H. H. Hng, X. W. (David) Lou, *J. Am. Chem. Soc.* **2012**, *134*, 17388.
[45] M. Shao, C. Li, T. Li, H. Zhao, W. Yu, R. Wang, J. Zhang, L. Yin, *Adv. Funct. Mater.* **2020**, *30*, 2006561.
[46] Y. Qian, B. Wu, Y. Li, Z. Pan, S. Feng, N. Lin, Y. Qian, *Angew. Chem. Int. Ed.* **2023**, *62*, e202217514.
[47] B. Wang, Z. Zhang, F. Yuan, D. Zhang, Q. Wang, W. Li, Z. Li, Y. A. Wu, W. Wang, *Chem. Eng. J.* **2022**, *428*, 131093.
[48] A. Ponrouch, P.-L. Taberna, P. Simon, M. R. Palacín, *Electrochim. Acta* **2012**, *61*, 13.
[49] H. Sun, G. Xin, T. Hu, M. Yu, D. Shao, X. Sun, J. Lian, *Nat. Commun.* **2014**, *5*, 4526.
[50] Y. Ma, Y. Ma, G. Kim, T. Diemant, R. J. Behm, D. Geiger, U. Kaiser, A. Varzi, S. Passerini, *Adv. Energy Mater.* **2019**, *9*, 1902077.
[51] A. Ponrouch, P.-L. Taberna, P. Simon, M. R. Palacín, *Electrochim. Acta* **2012**, *61*, 13.
[52] J. Wen, L. Xu, J. Wang, Y. Xiong, J. Ma, C. Jiang, L. Cao, J. Li, M. Zeng, *J. Power Sources* **2020**, *474*, 228491.
[53] C. Wang, Q. Wang, Y. Yu, J. Dai, *J. Mater. Sci. Mater. Electron.* **2024**, *35*, 1106.
[54] L. Hu, Y. Huang, F. Zhang, Q. Chen, *Nanoscale* **2013**, *5*, 4186.
[55] V. Augustyn, J. Come, M. A. Lowe, J. W. Kim, P.-L. Taberna, S. H. Tolbert, H. D. Abruña, P. Simon, B. Dunn, *Nat. Mater.* **2013**, *12*, 518.
[56] F. Zeng, W. Cheng, Y. Pan, M. Yu, Y. Qu, C. Yuan, *J. Mater. Chem. A* **2020**, *8*, 23919.

Manuscript received: December 11, 2024
Revised manuscript received: February 14, 2025
Accepted manuscript online: February 18, 2025
Version of record online: March 5, 2025

© 2025 Wiley-VCH GmbH

25666223, 2025, 8, Downloaded from https://chemistry-europe.onlinelibrary.wiley.com/doi/10.1002/batt.202400779 by University of Ulsan, Wiley Online Library on [11/11/2025]. See the Terms and Conditions (https://onlinelibrary.wiley.com/terms-and-conditions) on Wiley Online Library for rules of use; OA articles are governed by the applicable Creative Commons License